Influence of stress correlations on dislocation glide in random alloys

Ali Rida, Enrique Martinez, David Rodney, Pierre-Antoine Geslin

Influence of stress correlations on dislocation glide in random alloys

Ali Rida
Univ. Lyon, INSA Lyon, CNRS, UCBL, MATEIS, UMR5510, 69621 Villeurbanne, France

Enrique Martinez
Department of Mechanical Engineering, Clemson University, Clemson, SC 29623, USA and Department of Materials Science and Engineering, Clemson University, Clemson, SC 29623, USA

David Rodney*
Univ. Lyon, Université Claude Bernard Lyon 1, CNRS, UCBL, Institut Lumière Matière, UMR5366, 69622 Villeurbanne, France

Pierre-Antoine Geslin†
Univ. Lyon, INSA Lyon, CNRS, UCBL, MATEIS, UMR5510, 69621 Villeurbanne Cedex, France

Link to the article on the APS website: https://doi.org/10.1103/PhysRevMaterials.6.033605

Solute strengthening is an important mechanism that contributes to improving the mechanical properties of alloys and particularly the recent generations of concentrated alloys. The stress field emerging from an elastic model of a random solid solution displays strongly anisotropic correlations that interact differently with dislocations of different characters. In the present work, we investigate the depinning transition of edge and screw dislocations evolving in such a correlated stress environment using a dislocation dynamics numerical model. We find that edge dislocations are only weakly affected by the correlations, while screw dislocations are strongly influenced, showing a smaller critical stress, which increases with the amplitude of the stress noise with a larger exponent than the edge dislocation. The numerical results are compared with existing statistical models of solute strengthening, allowing to discuss critically their assumptions.

I. INTRODUCTION

Solid solution strengthening largely contributes to improving the mechanical properties of alloys [1]. The random distribution of solute elements raises obstacles for dislocation glide, therefore increasing the material's yield stress. Highly-concentrated alloys such as high entropy alloys, have attracted an increasing attention over the past decade and take full advantage of solute strengthening to reach exceptional mechanical properties [2, 3]. Considering the large composition space to explore, designing and optimizing these alloys require predictive and reliable models of solute strengthening that need to rely on well-controlled assumptions [4–6]. Atomistic calculations such as molecular dynamics provide an informative tool to investigate dislocation/solute interactions [7–11]. However, these simulations remain limited by the availability of reliable interatomic potentials and by intrinsic limitations in terms of length and time-scales.

Solid solution strengthening is best approached at the mesoscale considering the glide of an effectively infinite dislocation in a random distribution of solutes. This configuration is at the basis of the historical models of solute strengthening, which introduced a statistical treatment of the dislocation/solute interactions. In the Friedel - Fleischer approach, the dislocation bows out between well-separated obstacles [12, 13], limiting the model to the dilute regime. The Nabarro-Mott-Labusch approach, developed through a series of articles [14–16], proposes a statistical treatment valid for concentrated solid solutions, by summing the contribution of all solutes interacting with a dislocation segment.

In recent contributions [17, 18], the group of William Curtin has revisited the Nabarro-Mott-Labusch statistical treatment using the interaction energy between a straight dislocation and solute atoms instead of the force profile considered in the original approaches. A strength of this more recent model is that the interaction energy can be obtained either analytically if the solutes are described as elastic inclusions, or numerically from atomistic calcu-

* david.rodney@univ-lyon1.fr
† pierre-antoine.geslin@insa-lyon.fr

lations (either relying on empirical potentials or *ab initio*) to incorporate short-ranged non-linear core effects in addition to the long-range elastic interactions. This approach has been applied to various systems and yield quantitative estimates in both the dilute and concentrated limits [17–20].

Solid solution strengthening is also connected to the more theoretical literature on the depinning transition [21]. Indeed a dislocation gliding through a distribution of solute atoms can be seen as an elastic line evolving in a random quenched noise, a statistical physics framework that finds a wide range of applications, such as surface growth [22], fluid flow in porous media [23] or the propagation of a crack front in brittle fracture [24]. In most studies, the authors consider a quenched noise either fully uncorrelated or with short-ranged correlations [25–31]. Also, long-range elastic interactions along the line are often neglected by using a line tension approximation for the line stiffness. In such a case, i.e. a one-dimensional interface evolving in an isotropic and short-ranged correlated noise, a simple scaling argument originating from Larkin [32, 33] reveals a characteristic length-scale and deduce that the critical driving force to unpin the interface is proportional to the variance of the underlying noise elevated to the 2/3 power, a result consistent with the Nabarro-Mott-Labusch approach that also relies on a single characteristic length-scale [15, 16, 18, 19]. The spatial correlations of the underlying noise are known to influence the depinning transition [24, 34], although they have been mostly studied in the context of non-equilibrium surface growth phenomena and kinetic roughening [35–39]. We note that the depinning transition framework has been applied to the study of dislocations, but using isotropically short-ranged correlated stress environments that lack physical justification [33, 40].

In previous contributions [41, 42], we investigated the statistical properties of the stress field emerging from concentrated random solid solutions. Atoms were represented as dilatation and compression centers in an average isotropic elastic medium. We point out that this elastic model only accounts for atomic size mismatch and does not incorporate the potential role of spatially varying elastic constants or chemical interactions between species that may also contribute to solute strengthening. The atomic size differences were modeled with eigenstrains distributed around the lattice positions with a small-scale regularization parameter a, which was found close to 1 Å to match atomistic calculations [41]. Within the linear elasticity theory, the variance of both the resolved shear stress acting on a dislocation, $\langle \tau_p^2 \rangle$, and of the atomic displacements, $\langle u^2 \rangle$ (the so-called lattice distortion [43]), were shown proportional to the variance of the eigenstrains defined as $\langle \varepsilon^2 \rangle = \sum_i c_i \varepsilon_i^2$ (with c_i and ε_i, respectively the concentration and eigenstrain of element i). This quantity reduces to the square of the classical size mismatch parameter, δ^2 [44], if the alloy satisfies Vegard's law: $\langle \tau_p^2 \rangle \sim \langle u^2 \rangle \sim \sum_i c_i \varepsilon_i^2 \sim \delta^2$ [41]. More strikingly, we demonstrated in Ref. [42] that the shear stress field in the glide plane of a dislocation displays anisotropic correlations, expressed in polar coordinates as $\Sigma(d,\theta) = \Sigma_L(d)\sin^2(\theta) + \Sigma_T(d)\cos^2(\theta)$, where

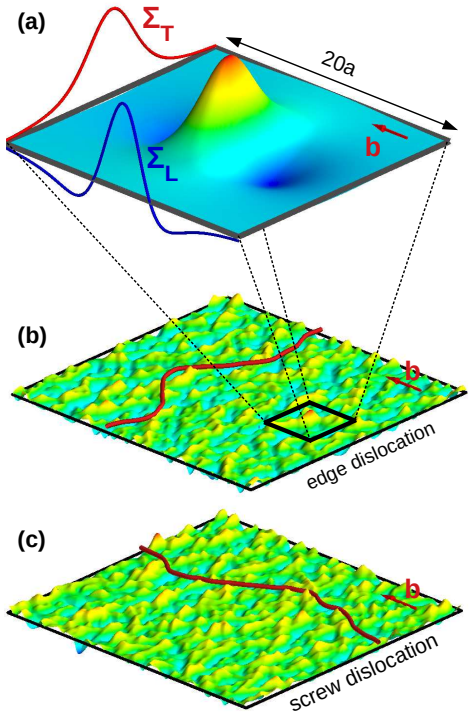

FIG. 1: Anisotropy of shear stress autocorrelations: (a) 2D autocorrelation function of the resolved shear stress acting in the glide plane of a dislocation of Burgers vector $\boldsymbol{b}$. The blue and red lines represent the correlation functions along the principal axes, parallel (Σ_L, Eq. (1)) and perpendicular (Σ_T, Eq. (2)) to $\boldsymbol{b}$. (b-c) Examples of edge and screw dislocations relaxed in random stress fields presenting the anisotropic correlations depicted in panel (a).

$$\Sigma_L(d) = -30\left(\frac{a}{d}\right)^3\left[\sqrt{\pi}\left(1-\frac{12a^2}{d^2}\right)\mathrm{erf}\left(\frac{d}{2a}\right)+\frac{a}{d}\left(12+\frac{d^2}{a^2}\right)\exp\left(-\frac{d^2}{4a^2}\right)\right], \quad (1)$$

$$\Sigma_T(d) = 15\left(\frac{a}{d}\right)^3\left[\sqrt{\pi}\left(1-\frac{6a^2}{d^2}\right)\mathrm{erf}\left(\frac{d}{2a}\right)+\frac{6a}{d}\exp\left(-\frac{d^2}{4a^2}\right)\right]. \quad (2)$$

We note that, in contrast to the convention of Ref. [42], Σ_L and Σ_T denote here normalized correlation functions, i.e. with $\Sigma_L(0) = \Sigma_T(0) = 1$. In the above equations, Σ_L is the autocorrelation of the shear stress field in the direction of the shear, i.e. along the principal axis parallel to the dislocation Burgers vector, while Σ_T denotes the autocorrelation in the transverse direction perpendicular to the Burgers vector. Both functions, as well as the resulting two-dimensional autocorrelation map are shown in Fig. 1.a. Correlations are strongly anisotropic, with the transverse correlations being uniformly positive, while the longitudinal correlations are negative at long range. We also note that $\int_{-\infty}^{+\infty}\Sigma_L(x)dx = 0$, the physical interpretation of which will be discussed. Finally, we highlight the power-law behavior of the correlations at long distance: for $d \gg a$, $2\Sigma_T(d) = -\Sigma_L(d) \sim \frac{1}{d^3}$. This scaling is expected for a random isotropic medium [45] but differs from the isotropic short-ranged correlations generally assumed in the literature as noted above.

Since the depinning transition is known to depend on the correlations of the underlying structural noise, it becomes of upmost importance to evaluate the effect on dislocation glide of the anisotropic correlations evidenced in random alloys. Moreover, since edge and screw dislocations lie respectively mostly along the transverse and longitudinal directions, one can expect a different effect of the correlations on both dislocation characters. As illustrated in Figs. 1.b and c, we have used an elastic model and performed dislocation dynamics simulations for both edge and screw dislocations in correlated random stress environments, as well as in an isotropic uncorrelated noise as considered previously in the literature. The simulations are performed in the limit of zero temperature by increasing the applied stress quasistatically and using a quenched noise. We thus assume in particular that the diffusional time of the solutes is large compared the glide time of the dislocations. We find that the edge dislocation is not significantly affected by the correlations, with a critical shear stress showing a 2/3-exponent independently of whether long-range elasticity or a simple line tension approximation are used to represent the dislocation energetics. However, the screw dislocation follows a different behavior, with a lower critical shear stress, which increases with the noise amplitude with a larger exponent. The numerical simulations are analyzed using both the classical force-based model developed by Larkin [32] and the more recent energy-based model developed in Curtin's group [17, 18]. We will see that, while both models reproduce the 2/3 exponent of the edge dislocation, they fail to reproduce the greater exponent of the screw dislocation. The hypotheses and approximations of both models are critically discussed.

II. DISLOCATION MODELING

The dislocation is represented by an L-periodic time-dependent function $h(x,t)$ (x is the coordinate along the dislocation direction and t the time) gliding in a periodic environment of dimensions $L \times L$ (see Fig. 2). In the following, y and z respectively denote the glide direction and the normal to the glide plane. We describe its dynamics using a dissipative equation of motion:

$$B\partial_t h(x,t) = -\frac{\delta E[h]}{\delta h} + b\tau_p(x,h(x,t)) + b\tau_a, \quad (3)$$

where B is a drag coefficient characteristic of the viscous motion of the dislocation and b is the norm of dislocation Burgers vector. The right-hand side of Eq. (3) contains the forces acting on the dislocation: (i) the self-force, expressed as the functional derivative of the dislocation self-energy E with respect to the dislocation height, (ii) the pinning force due to the random stress field, i.e. the Peach-Koehler force generated by the shear stress due to the solutes at the dislocation position, $\tau_p(x,h(x,t))$, and (iii) the Peach-Koehler force due to the external applied stress τ_a. We discuss below how the forces (i) and (ii) are computed numerically.

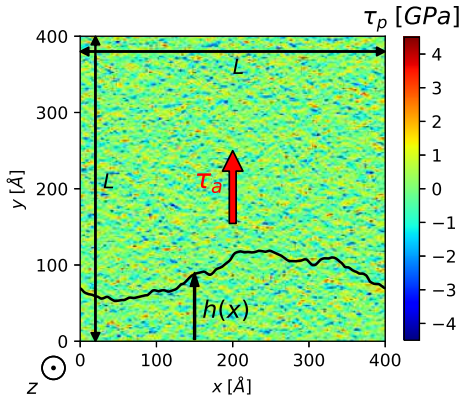

FIG. 2: Simulation setup for a dislocation gliding in a square periodic cell of length $L = 400$ Å.

A. Equation of motion in Fourier space and dislocation self-energy

The dislocation self-energy $E[h]$ is written as a functional of its height h and can account for long-range elastic interactions characteristic of dislocations using the non-singular dislocation theory of Cai et al. [46]. It allows to regularize the divergence of elastic fields at the dislocation core by spreading the Burgers vector in space over a small distance a_{NS}. Using this dislocation model, it has been shown in Ref. [47] that in the limit of small perturbation $|\partial_x h| \ll 1$, $E[h]$ can be expressed analytically as a function of the Fourier amplitudes of h, such that, in Fourier space, Eq. (3) becomes a set of coupled differential equations:

$$B\partial_t \widehat{h}(k) = -\Gamma(k)k^2\widehat{h}(k) + b\widehat{\tau_p[h]}(k) + b\tau_a\delta(k), \quad (4)$$

where k denotes the wave vector and $\hat{f}(k)$ are the Fourier amplitude of $f(x)$. From this equation, we see that long-range elasticity is simply incorporated as a k-dependent line tension, $\Gamma(k)$, which is expressed as follows for edge and screw dislocations (see Ref. [47] for details):

$$\Gamma_e(\bar{k}_e) = \Gamma_e^{co} + \frac{\mu b^2}{2\pi(1-\nu)\bar{k}_e^2}\left[-1 - \nu\bar{k}_e^2 K_0(\bar{k}_e) - \bar{k}_e K_1(\bar{k}_e)\left(1 - \frac{\bar{k}_e^2(1-\nu)}{2}\right) + \bar{k}_e K_2(\bar{k}_e)\right] \quad (5)$$

$$\Gamma_s(\bar{k}_s) = \Gamma_s^{co} + \frac{\mu b^2}{2\pi(1-\nu)\bar{k}_s^2}\left[-2(1-\nu) + 2\bar{k}_s^2 K_0(\bar{k}_s) + (3-\nu)\bar{k}_s K_1(\bar{k}_s) - \frac{1+\nu}{2}\bar{k}_s^2 K_2(\bar{k}_s)\right] \quad (6)$$

where $\bar{k}_s = ka_{NS}^s$ and $\bar{k}_e = ka_{NS}^e$ are dimensionless wave-vectors normalized by the regularization length of the non-singular theory [46], which we assume character-dependent. K_0, K_1 and K_3 are Bessel functions of the second kind and μ and ν denote the Lamé elastic parameters of the isotropic elastic medium. These expressions translate the fact that the edge and screw dislocations become stiffer on longer wave-lengths. For both edge and screw dislocations, the core line tensions Γ_s^{co} and Γ_e^{co} and the non-singular parameters a_{NS}^s and a_{NS}^e have been determined from atomistic calculations in the case of pure Al using the capillary fluctuation method [47]. Their numerical values are given in Tab. I.

The dislocation model might be simplified and long-range elasticity may be neglected by using a line tension approximation. With this approximation, the self-force of Eq. (3) reduces to $-\frac{\delta E[h]}{\delta h} = -\Gamma\frac{\partial^2 h}{\partial x^2}$. In Fourier space, this translates into Eq.(4) where Γ is now a constant independent of the wave vector k. To determine the specific values of the line-tension for the screw and edge characters, we use Eq.(5-6) and chose $\Gamma = \Gamma(k_0)$ where k_0 corresponds to a typical wavelength of 100 Å. The corresponding values are also given in Tab. I.

B. Correlated noise

To generate a correlated structural noise, $\tau_p(x, y)$, we discretize space on a regular square grid of size $N \times N$ with a spacing $\Delta x = L/N$. In practice, all simulations were performed with $\Delta x = 0.5$ Å $\simeq a/2$, which is small enough to describe the spatial correlations of the stress field expressed in Eqs.(1-2). The correlated noise is generated on the grid using a spectral method presented in Refs. [48, 49] and outlined below.

Based on the microelastic model developed in Refs. [41, 42], the autocorrelation of a shear stress component τ_{mn} $(m \neq n)$ is expressed in Fourier space for a system of dimensions L_x, L_y and L_z as:

$$\widehat{\Sigma}_{mn}(k_x, k_y, k_z) = \frac{120\pi^{3/2}a^3}{L_x L_y L_z} \frac{k_m^2 k_n^2}{\boldsymbol{k}^4} e^{-a^2\boldsymbol{k}^2}. \quad (7)$$

The random amplitude of Fourier modes are then generated as:

$$\widehat{R}(k_x, k_y, k_z) = \sqrt{\frac{\widehat{\Sigma}_{mn}(k_x, k_y, k_z)}{2}}(N_k + iM_k), \quad (8)$$

where N_k and M_k are Gaussian random variables with mean 0 and standard deviation 1. As shown in Refs. [48, 49], the inverse Fourier transform of the above field follows a Gaussian distribution of variance 1 and appropriate correlations in 3D. Multiplied by $\sqrt{\langle \tau_p^2 \rangle}$, this field yields the quenched noise to be used in the simulations, with values between grid points obtained from quadratic interpolations.

A 3D field is needed with the non-singular theory because the dislocation core is spread in 3D (see below). We choose the same grid spacing Δx and a size $L_z = 64$ Å along the z direction, which is much larger than the regularizations parameter a and a_{NS}, and yields correlations representative of an infinite system along the z direction. With the line tension approximation, only the 2D field in the dislocation glide plane is needed. We can then either use a slab of the 3D field at constant z or perform the inverse Fourier transform of Eq. (7) in the z direction beforehand, considering an infinite system in this direction (see Eq. (A3)), in order to generate the appropriate correlations directly in 2D. The random stress environments obtained with both 2D and 3D methods are statistically equivalent.

Fig. 3 displays the correlations of the noise generated numerically with a comparison to the analytical expressions of Eqs. (1-2). The perfect agreement demonstrates the capability of the spectral method to generate correlated noises. Two realizations of the 2D random stress field are shown as illustrations in Fig. 1.b and c. The anisotropy of the stress field, inherited from the anisotropy of the correlations, is clearly visible in these figures with a succession of "mountains" (maxima) and "valleys" (minima) in the direction of the Burgers vector and a general alignment of the mountains (maxima) in the perpendicular direction. As mentioned above, it can be expected that edge and screw dislocations, which lie in

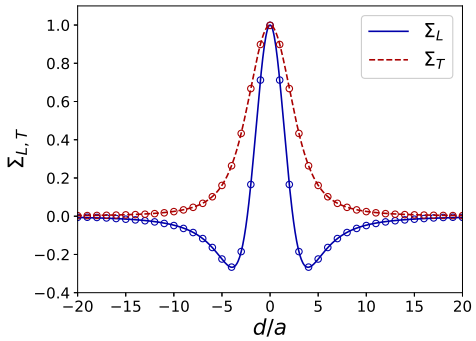

FIG. 3: Longitudinal and transverse correlations obtained from the spectral noise generator (symbols) and compared to the analytical expressions of Eqs. (1) and (2) shown with continuous and dash line respectively.

the transverse (Fig. 1.b) and longitudinal (Fig. 1.c) directions respectively, will be affected differently by this anisotropic structural noise.

To use the non-singular dislocation theory, the correlated noise environment needs to be convoluted in order to account for the fact that the dislocation Burgers vector is spread out radially around the dislocation line. The spreading function introduced in Ref. [46] is defined through its self-convolution:

$$(w * w)(\boldsymbol{r}) = \frac{15a_{NS}^4}{8\pi\left[\boldsymbol{r}^2 + a_{NS}^2\right]^{7/2}}. \quad (9)$$

The convolution of the pinning stress noise is performed in Fourier space by simply multiplying Eq. (8) by the Fourier transform of $w(\boldsymbol{r})$ expressed as:

$$\widehat{w}(k_x, k_y, k_z) = a_{NS}|\boldsymbol{k}|\sqrt{\frac{K_2(a_{NS}|\boldsymbol{k}|)}{2}}, \quad (10)$$

where K_2 denotes the second modified Bessel function of the second kind and $|\boldsymbol{k}| = \sqrt{k_x^2 + k_y^2 + k_z^2}$. After this convolution step, the noise is obtained in real space by an inverse Fourier transform.

C. Numerical integration and size effects

The critical shear stress is obtained using a quasistatic algorithm where the applied stress τ_a is increased in small increments of the order of 1% of the expected critical shear stress and the system is

relaxed at each increment. Equilibrium is found using a spectral method. The dislocation height is first discretized in real space using the same spacing Δx as the structural noise. The dislocation is then fully described by $\frac{N}{2}+1$ modes in Fourier space with wave vectors $k \in [0, \frac{2\pi}{L}, \ldots, \frac{\pi}{\Delta x}]$ and amplitudes $\widehat{h}_k = \frac{1}{N}\sum_{n=0}^{N-1} h(x_n) e^{-ikx_n}$. After discretization, Eq. (4) reduces to a set of $\frac{N}{2}+1$ coupled equations:

$$B\partial_t \widehat{h}_k = -\Gamma(k)k^2\widehat{h}_k + b\left[\widehat{\tau_p[h]}\right]_k + b\tau_a\delta_k, \qquad (11)$$

where $\delta_k = 1$ if $k = 0$ and 0 otherwise. Time is discretized with a time step Δt and Eq. (11) is integrated employing a semi-implicit method, where the linear term $\Gamma(k)k^2\widehat{h}_k$ is estimated at time $t+\Delta t$ while the stress $\tau_p[h]$ acting on the dislocation line is computed in real space at time t before being transposed to Fourier space. The integration scheme is written for each k vector as:

$$\widehat{h}_k^{t+\Delta t} = \frac{\widehat{h}_k^t + \frac{\Delta t}{B} b\left(\left[\widehat{\tau_p[h^t]}\right]_k + \tau_a\delta_k\right)}{1+\frac{\Delta t}{B}\Gamma(k)k^2}. \qquad (12)$$

The different quantities are normalized using the characteristic length $l_c = b$, characteristic stress $\sigma_c = \Gamma/b^2$ and characteristic time $t_c = Bb^2/\Gamma$, where Γ is the dislocation line tension (the core line tension Γ^{co} was used with the non-singular theory). The time step is set to $\Delta t = 0.1t_c$, which ensures the stability of the algorithm while allowing for a fast convergence. Integration is stopped when the right-hand side of Eq. (11) becomes smaller than the dimensionless threshold $f_{th} = 10^{-10}$ for all the Fourier modes.

When the applied stress is larger than the critical stress, the semi-implicit algorithm fails to find an equilibrium and the dislocation glides indefinitely through the periodic simulation cell. We define the critical stress as the largest stress at which Eq. (11) converged to an equilibrium. To reach representative statistics, critical stresses were averaged over 100 simulations performed with different random pinning stress fields. We have checked that the results are converged with respect to the grid spacing Δx, the time step Δt and the threshold f_{th}. The other parameters used in the simulations are listed in Tab. I.

Calculations of critical shear stresses are known to exhibit finite-size effects [50, 51]. Using a square cell partly mitigates these effects, but, as shown in Fig. 4, the calculated critical stresses still depend significantly on the simulation cell size. The dependence can be fitted as an exponential function of the system size L. We therefore performed simulations in cells of increasing lengths and used exponential fits to extrapolate to infinite systems. Note that even if the convergence is exponential, the size effect is significant. For instance, using a small cell of length $L = 200$ Å typical of atomistic calculations, the critical shear stress of an edge dislocation is overestimated by $10-20\%$ compared to the infinite-system limit.

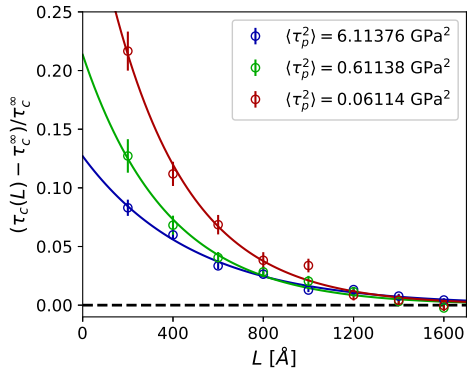

FIG. 4: Finite-size effects on the critical shear stress of an edge dislocation as a function of the system size L for three different noise variances $\langle\tau_p^2\rangle$. Error bars denote the uncertainty on the value averaged over 100 realizations. Continuous lines are exponential fits.

III. RESULTS WITH THE NON-SINGULAR DISLOCATION MODEL

A. Dislocation relaxation in a random alloy

To assess the capability of the elastic model to describe dislocations in concentrated alloys, we first compare its predictions with atomistic simulations performed in a binary Al-Mg system modeled with the interatomic potential of Ref. [52], which was already employed in our previous work [41, 42].

1. *Elastic model*

For the elastic model, we used the parameters listed in Tab. I, which correspond to an $Al_{50}Mg_{50}$

Symbol	Value	Unit
$\bar{a}_{lat}$	4.282	Å
μ	20.7	GPa
ν	0.331	–
$\langle \tau_p^2 \rangle$	0.6114	GPa^2
a	1.0355	Å
a^s_{NS}	3.34	Å
a^e_{NS}	5.60	Å
Γ^{co}_s	0.114	eV/Å
Γ^{co}_e	0.053	eV/Å
Γ_s (LT)	0.3424	eV/Å
Γ_e (LT)	0.1296	eV/Å
Δx	0.5	Å

TABLE I: Parameters used to model a $Al_{50}Mg_{50}$ alloy. The non-singular parameters and core line tension were determined for edge and screw dislocations in pure Al in Ref. [47]. The spreading parameter a and noise variance $\langle \tau_p^2 \rangle$ were determined for $Al_{50}Mg_{50}$ in Ref. [41].

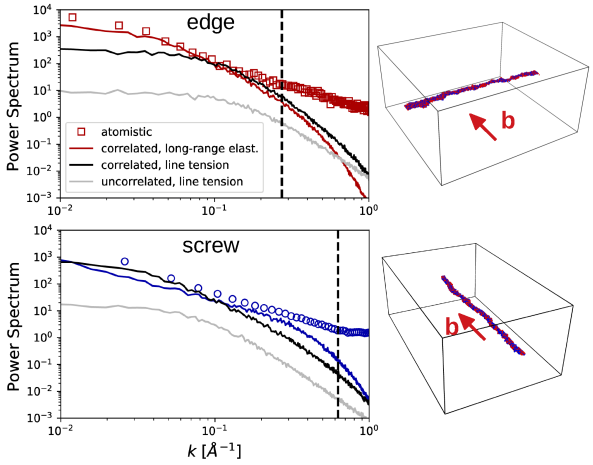

FIG. 5: Left column: Power spectra obtained from atomistic calculations (symbols) and with the elastic model relying on different assumptions concerning the nature of the underlying noise (uncorrelated or correlated) and the dislocation model (long-range elasticity or line tension approximation). Right column: atomistic simulations of relaxed edge and screw dislocations in $Al_{50}M_{50}$ alloy (only defected atoms belonging to the dislocation cores are shown).

random alloy. We considered both correlated and uncorrelated noises and used both the non-singular dislocation theory and the line tension approximation. Initially straight dislocations were relaxed in random noises with no applied stress and Fourier transforms were performed to obtain the power spectra of the equilibrium dislocation shapes, which were averaged over 100 realizations.

The result is shown in Fig. 5, which compares the power spectra of edge and screw dislocations obtained with different approximations: (i) uncorrelated noise and line tension approximation (grey lines), (ii) correlated noise and line tension approximation (black lines) and (iii) correlated noise and long-range elasticity accounted for in the non-singular theory (red and blue lines). We see that both noise correlation and long-range elasticity influence significantly the results. In particular, both effects contribute to change the slope of the power spectra. Correlations increase the amplitude of the long wavelength modes of both the edge and screw dislocations. Long-range elasticity also increases the amplitude of these modes for the edge dislocation, while it has a weaker effect on the screw character. We note that the convolution of the pinning stress with the spreading function of the non-singular theory averages locally the noise and modifies its correlations in a non-trivial way that depends on the ratio a/a_{NS} between the spreading lengths. This effect, added up to the change of dislocation line tension with k embedded in Eqs. (5-6), explains the difference between the black and colored lines in Fig. 5. Note that without applied stress, all power spectra tend to converge to a constant value for small wave vectors, an effect that will be clarified in Section V B.

2. *Comparison with atomistic calculations*

In the atomistic calculations, a dislocation is introduced in a random $Al_{50}Mg_{50}$ alloy. The atomistic cells have dimensions $523.6 \times 485.2 \times 250.4$ Å^3 and $478.0 \times 311.8 \times 195.5$ Å^3 for the edge and screw characters, respectively. To overcome the small Peierls barriers against dislocation motion in this alloy and allow the dislocation to relax to a stable minimum, the system is thermalized at 300 K for 10 ps before quenching. All atomistic calculations are performed with the Lammps software [53] and the dislocation position $h(x)$ is extracted from the atomic configurations by averaging the position of stacking fault atoms detected by the common neighbor analysis tool of Lammps. Averaged power spectra were obtained from 50 independent configurations and are shown with open symbols in Fig. 5. The vertical

dashed lines represent the characteristic wave vector $k_{th} = 2\pi/d_0$ corresponding to the dissociation distance d_0 between Shockley partials. Above this threshold, the elastic model is expected to fail to reproduce atomistic results since it does not incorporate dissociated dislocation cores. Below k_{th} on the other hand, Fig. 5 shows that the elastic model reproduces the atomistic results fairly well if a correlated noise and the non-singular dislocation description are used (red and blue lines). It is worth highlighting that this agreement is obtained without any adjustable parameter.

B. Critical shear stress

1. *Elastic model*

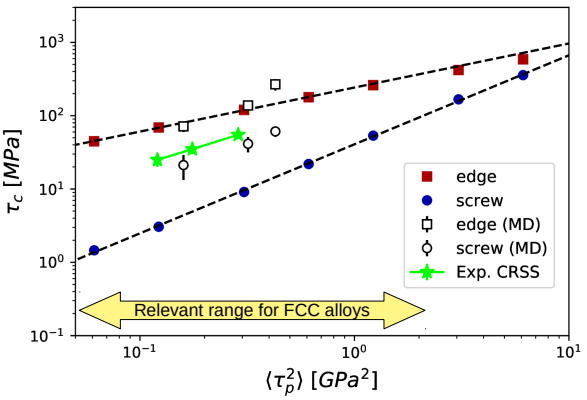

FIG. 6: Critical shear stress of edge and screw dislocations modeled with the non-singular dislocation theory in correlated noises of varying amplitude. The dashed lines represent fits to power laws with different exponents (see text). Open symbols were obtained from atomistic calculations. Green stars represent experimental data obtained at $T < 10$ K on monocystalline Al-Mg alloys of concentrations $c_{Mg} = 3.78$ %, 5.52 % and 9 % [54]

We then use the elastic model to compute the critical shear stress of edge and screw dislocations for various strengths of the pinning field, thus corresponding to solid solutions of different eigenstrain variances. Fig. 6 shows in a log-log plot the values of the critical shear stress (extrapolated to infinite systems as explained in section II C) as a function of the variance of the pinning field $\langle\tau_p^2\rangle$. For reference, experimental data obtained for Al-Mg alloys of various concentrations are shown as green stars; the amplitude of $\langle\tau_p^2\rangle$ is deduced from the concentrations using our elastic model [41]. More generally, the range of amplitudes typical of face-centered cubic concentrated alloys is represented with a yellow arrow in Fig. 6. This range is deduced from the values of the misfit parameter and elastic constants measured in various alloys [19, 41, 55].

The critical stress of both screw and edge dislocations tends to follow power laws with different exponents. Numerical fits ($\tau_c \sim \langle\tau_p^2\rangle^\alpha$) shown as dashed lines in Fig. 6 yield exponents $\alpha_e = 0.601 \pm 0.007$ and $\alpha_s = 1.21 \pm 0.013$ for the edge and screw dislocations respectively. For the edge case, the exponent is close to 2/3, as obtained in previous works using a line tension approximation and an uncorrelated noise (see Refs. [21, 33, 40] and Section IV B). The numerical results show a slight deviation from the power-law behavior at high values of $\langle\tau_p^2\rangle$, which could be due to the long-range elasticity or the stress correlations. The screw dislocation has a significantly lower critical stress but an exponent about twice that of the edge dislocation. Screw dislocations are known to interact with substitutional solutes less than edge dislocations. A limiting case is an infinite straight screw dislocation, which has zero elastic interaction with dilatational solutes [56]. Within the present approach, this property is embedded in the statistical properties of the stress noise through the fact that $\int \Sigma_L(x)dx = 0$ (see section V). At low pinning amplitudes, the screw dislocation remains almost perfectly straight and has thus a negligible critical stress. However, as the pinning stress amplitude increases, the dislocation bows out increasingly to avoid stress peaks, thus acquiring locally a non-screw character that interacts with the solute field. As a result, the critical shear stress increases rapidly with the pinning amplitude, with an apparent exponent greater than the edge dislocation that has a finite critical stress even when perfectly straight.

2. *Comparison with atomistic and experimental results*

Results from quasistatic atomistic calculations are shown as black symbols in Fig. 6. The composition range explored here is $5\% - 15\%$ because simulations with higher Mg contents led to significant core effects such as local constrictions and cross-slip of screw segments as observed in high-entropy alloys [57]. The critical shear stress was averaged over 50 realizations and the Peierls stress of pure Al was subtracted as it is not incorporated in the elastic model.

The critical shear stress obtained for the edge dislocation agrees well with the elastic model at 5 and 10%, which correspond respectively to $\langle \tau_p^2 \rangle = 0.16$ and $0.32\,\mathrm{GPa}^2$. At 15% (i.e. $\langle \tau_p^2 \rangle = 0.43\,\mathrm{GPa}^2$), core effects start to affect the critical stress and the atomistic data is larger than with the elastic model. For the screw dislocation, the atomistic simulations systematically overestimate the elastic model. The main reason is probably that in atomistic simulations, the dislocation core is dissociated into partials with an edge component which interact more strongly with the solutes than the single screw core assumed in the elastic model. Also, the anelastic interactions of the solutes with the dislocation core and stacking fault that are neglected in the elastic model may contribute to solute strengthening in the atomistic calculations. We note however that, although the atomistic data span less than a decade in $\langle \tau_p^2 \rangle$, the atomistic screw critical stress displays an exponent larger than 2/3, in agreement with the elastic model.

These results can also be compared to the atomistic calculations of Patinet and Proville [9] performed in Al-Mg but with a different interatomic potential. They found that the critical shear stress of the edge dislocation follows approximately a 2/3 exponent as observed here. For the screw dislocation, they also found a lower critical stress and a larger exponent, although the exponent found in their study is close to 1 and thus slightly smaller than the one evidenced by numerical results in Fig. 6.

Interestingly, results from both the elastic model and atomistic simulations are qualitatively consistent with experimental measurements taken from Ref. [54] and shown as green stars in Fig. 6: as expected, the experimental data fall between the results obtained for the edge and the screw dislocations with both modeling techniques.

This section demonstrates how our spectral dislocation dynamics method can be used to model non-singular dislocations in the correlated stress environment emerging from a random solid solution. These findings however lack generality and rely on a number of potentially interfering material and numerical parameters, such as the a/a_{NS} ratio. It is therefore difficult to generalize the present findings to a larger class of alloys. For this reason, we have also performed calculations using a line tension approximation. As already seen in Fig. 5, this approximation influence slightly the power spectra if a correlated noise is used. Moreover, we will see in the following that the same applies to the critical resolved shear stress. The line tension approximation also holds the advantage of allowing for an analytical analysis that can be compared to models from the literature, which generally also neglect long-range elastic interactions along the dislocation.

IV. RESULTS WITH THE LINE TENSION APPROXIMATION

A. Numerical results

In the present framework, the line tension approximation consists in considering Γ constant in Eq. (4). Its specific value is unimportant because Eq. (4) can be re-written in an dimensionless form independent of Γ, by rescaling stresses by Γ/b^2 and lengths by b. Time is rescaled by b^2B/Γ but does not play a physical role in the present quasistatic calculations.

Following the same methodology as described in section II C, the critical shear stresses obtained with the line tension approximation are presented in Fig. 7 with both correlated or uncorrelated noises. In the case of an isotropic uncorrelated noise (black diamond symbols in Fig. 7), edge and screw dislocations are equivalent if dimensionless stresses are used and we recover the expected 2/3 exponent. If correlations are accounted for, the results are comparable to those obtained with the non-singular dislocation theory: at low pinning stress, the edge dislocation still follows a power-law with an exponent $\alpha_e = 0.6 \pm 0.006$ close to the expected value of 2/3. We note however that the screw dislocation no longer follows a single power law, but has an exponent $\alpha_s = 1.367 \pm 0.024$ at low pinning amplitude, which decreases towards a value close to 2/3 at higher pinning amplitudes, similar to the edge and uncorrelated cases.

We thus see that the line tension approximation recovers at least qualitatively the same results obtained with the non-singular dislocation model. It allows for an analytical treatment described below.

B. Force-based model

The above numerical results can be rationalized by extending the statistical treatment first proposed by Larkin [32] and Labusch [15] and widely used in the literature [21, 33, 40]. The central assumption is that dislocation unpinning is controlled by a single characteristic length-scale, λ_c (the so-called Larkin or Labusch length) that marks the transition between a regime dominated by the random stress

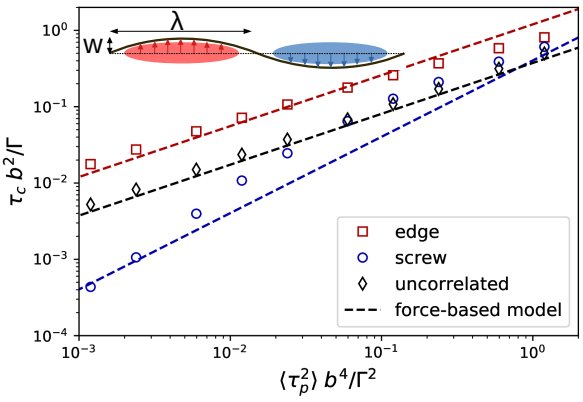

FIG. 7: Critical shear stress of edge and screw dislocations modeled with a line tension approximation. Numerical simulations are shown as symbols for correlated stresses corresponding to edge (□) and screw (◯) dislocations and for an uncorrelated stress field (◊). Dashed lines are predictions Eqs. (15-17) of the force-based model.

field ($\lambda > \lambda_c$) and a regime dominated by the line-tension contribution ($\lambda < \lambda_c$). The shape of the dislocation is then assimilated to a periodic function of the form $h(x) = w\sin(\pi x/\lambda_c)$. Upon relaxation, the dislocation moves in the glide direction until it finds a favorable local stress environment that balances the line tension. At equilibrium, the amplitude w is therefore associated with the characteristic length scale of the quenched noise in the glide direction [21, 40]. We assume here that w corresponds to the distance where the correlation functions drop below 1/2. From Eqs. (1-2), we found $w_e = 1.3898a$ and $w_s = 2.6969a$ for the edge and screw dislocations and we set $w_u = 0.5\Delta x$ for the uncorrelated noise.

To determine λ_c, we first integrate Eq. (3) with no applied stress over a distance λ_c (see inset in Fig. 7). This pinning force from the random stress environment should at equilibrium be compensated by the line tension force, yielding the condition:

$$\frac{2\pi\Gamma w}{\lambda_c} = b\int_0^{\lambda_c}\tau_p(x,h(x))dx, \tag{13}$$

where $\int_0^{\lambda_c}\tau_p(x,h(x))dx$ is a random variable that can be replaced by its standard deviation, $\sigma_\tau(\lambda_c)$. As a first approximation, we neglect the decay of the stress correlation in the glide direction between $h = 0$ and $h = w$, allowing to compute $\sigma_\tau(\lambda_c)$ along an unrelaxed straight dislocation:

$$\begin{aligned}\sigma_\tau(\lambda_c) &= \sqrt{\int_0^{\lambda_c}\int_0^{\lambda_c}\langle\tau_p(x,0)\tau_p(x',0)\rangle dxdx'} \\ &= \sqrt{\langle\tau_p^2\rangle\int_0^{\lambda_c}\int_0^{\lambda_c}\Sigma(x-x')dxdx'},\end{aligned} \tag{14}$$

where $\Sigma(x-x')$ is the shear stress autocorrelation function along the straight dislocation line. It thus corresponds to the correlation functions introduced in Section I and depends on the dislocation character: $\Sigma_L(x-x')$ from Eq. (1) for a screw dislocation and $\Sigma_T(x-x')$ from Eq. (2) for an edge dislocation. In the uncorrelated case, $\sigma_\tau^u(\lambda_c)$ is obtained from the central-limit theorem. The standard deviations for the edge (σ_τ^e) and the screw (σ_τ^s) cases can be integrated analytically from Eqs. (1-2), yielding in the relevant limit $\lambda_c \gg a$:

$$\sigma_\tau^u(\lambda_c) \underset{\lambda_c\gg a}{=} \sqrt{\Delta x\lambda_c\langle\tau_p^2\rangle} \tag{15}$$

$$\sigma_\tau^e(\lambda_c) \underset{\lambda_c\gg a}{=} \sqrt{\frac{15\sqrt{\pi}}{4}a\lambda_c\langle\tau_p^2\rangle} \tag{16}$$

$$\sigma_\tau^s(\lambda_c) \underset{\lambda_c\gg a}{=} \sqrt{20a^2\langle\tau_p^2\rangle} \tag{17}$$

With these expressions, Eq. (13) can be solved to obtain the characteristic length λ_c for the three cases. Note that in the screw case, σ_τ^s is non-zero because the double integral involved in Eq. (17) is computed in a finite non-periodic domain. Had we assumed a λ-periodic stress environment as in Ref. [18], the double integral would have been zero. This translates within the force-based model the fact that an infinite straight dislocation does not interact with dilatational solutes.

With λ_c known from Eq. (13), it is assumed that the force $b\sigma_\tau(\lambda_c)$ is the characteristic resistance due to the pinning stress field, which must be overcome by the applied stress, i.e. $\tau_c b\lambda_c = b\sigma_\tau(\lambda_c)$, which yields for all three cases:

$$\tau_c^u = \left(\frac{\Delta x}{\sqrt{2\pi}}\right)^{2/3}\left(\frac{b}{\Gamma w_u}\right)^{1/3}\langle\tau_p^2\rangle^{2/3} \tag{18}$$

$$\tau_c^e = \left(\frac{15a}{4\sqrt{2}}\right)^{2/3}\left(\frac{b}{\Gamma w_e}\right)^{1/3}\langle\tau_p^2\rangle^{2/3} \tag{19}$$

$$\tau_c^s = \frac{10a^2b}{\Gamma\pi w_s}\langle\tau_p^2\rangle \tag{20}$$

The predictions of these equations are shown as dashed lines in Fig. 7. Note that no parameter

was adjusted to obtain these results. For the uncorrelated noise, the analytical model predicts the expected 2/3 exponent known from the literature [21, 33, 40] and yields a quantitative prediction of the critical stress, very close to the numerical calculations. The same very good agreement is obtained with the edge dislocation. Eq. (19) predicts in particular that the edge dislocation should display the same 2/3 exponent as the uncorrelated case, in agreement with the numerical calculations. The mathematical reason is that the standard deviation σ_τ^e in Eq. (16) has the same square-root dependence on λ_c as σ_τ^u. Because the long-range correlations acting along the edge dislocation, i.e. Σ_T, are positive and integrable, the resulting noise is effectively equivalent to an uncorrelated noise defined on a grid of spacing $\Delta x = 15a\sqrt{\pi}/4$. In contrast, the force-based model predicts a different exponent for the screw dislocation. The negative correlations acting on the screw dislocation lead to a constant σ_τ^s independent of λ_c and in turn to a linear scaling $\tau_c \sim \langle \tau_p^2 \rangle$. The analytical model therefore predicts a lower exponent than the numerical calculations and fails to predict the variation of this exponent with pinning amplitudes.

At this point, it is valuable to convert the scaling obtained as function of the stress amplitude to a scaling as function of the alloy composition. The main parameter controlling the variance of the random noise $\langle \tau_p^2 \rangle$ is $\langle \varepsilon^2 \rangle = \sum_\alpha c_\alpha \varepsilon_\alpha^2$ [41]. If the alloy follows Vergard's law, its lattice spacing evolves linearly with composition: $\bar{a} = \sum_\alpha c_\alpha a_\alpha$, and $\langle \varepsilon^2 \rangle = \sum_\alpha c_\alpha \left(\frac{a_\alpha - \bar{a}}{\bar{a}}\right)^2$ evolves linearly with the compositions c_α in the dilute alloy limit $c_\alpha \ll 1$. Therefore, within these simplifying assumptions, the critical stress of the edge dislocation follows $\tau_p \sim \left[\sum_\alpha c_\alpha \left(\frac{a_\alpha - \bar{a}}{\bar{a}}\right)^2\right]^{2/3}$; we thus recover the scaling predicted by the Nabarro-Mott-Labusch approach [14–16], which is reassuring considering the similarities between this model and Larkin's model. Nevertheless, this scaling is rarely found in real alloys because of (i) deviations from Vegard's law, (ii) varying elastic constants with composition, (iii) the prevalence of chemical interactions and/or elastic constants heterogeneities over the size mismatch effect [58].

V. DISCUSSION

We have seen that accounting for the spatial correlations emerging from a random solid solution does not strongly affect an edge dislocation, whose critical stress follows a scaling law with the same 2/3 exponent as for an uncorrelated noise. Screw dislocations on the other hand are much more affected because the stress noise encodes through the property $\int \Sigma_L(x)dx = 0$ that a straight infinite screw dislocation does not interact with a field of dilatational solutes. Indeed, the absence of interaction implies that $\int \tau_p(x,0)dx = 0$ for a screw dislocation and thus $\int \Sigma_L(x)dx = \int \langle \tau_p(0)\tau_p(x)\rangle dx = \langle \tau_p(0) \int \tau_p(x,0)dx \rangle = 0$. The fact that Σ_L is negative at long distance while Σ_T remains positive therefore results from the fact that a screw dislocation does not interact with dilatational solutes while an edge dislocation does.

We have attempted to rationalize the simulation results using a classical force-based model. While the model applies well to the edge dislocation and correctly reproduces the fact that the screw dislocation has a lower critical stress, it fails to predict the correct exponent for the screw dislocation, even at low pinning amplitudes where the dislocation is mostly straight. This can be due to different simplifying assumptions of the force-based model that are listed below:

(i) The amplitude of the dislocation perturbation w is determined from ad-hoc considerations and is assumed small enough that the stress along the dislocation does not depend on the perturbation $h(x)$.

(ii) The critical stress is controlled by a single length scale λ_c while the dislocation shape involves all length scales (see Fig. 5).

(iii) The critical length scale λ_c is considered the same at 0 applied stress and at τ_c while the dislocation significantly roughens between these two states.

To try to improve the model predictions, we have first considered point (i) and used the energy-based model developed in Curtin's group [17, 18], which allows to predict the value of the amplitude of the dislocation perturbation w. This will be addressed in Section V A. In section V B, assumptions (ii) and (iii) - that are central to both force-based and energy-based models - are discussed in light of the power spectra of the dislocations that evolve significantly between 0 stress and the critical shear stress τ_c due to roughening.

A. Comparison with an energy-based model

One weakness of the force-based model presented above is that the amplitude of the dislocation perturbation, w, is not predicted by the model but needs to be set *a priori*. In section IV, we used the distance over which the stress correlations decrease by a factor 1/2 but other choices are possible. One advantage of the energy-based model developed in Curtin's group [17, 18] is to determine w from a minimization condition. We will thus compare in the following the predictions of the force-base model with Curtin's model in the case where the interaction energy between the dislocation and the solute atoms are elastic, as considered in Ref. [18]. We note that one assumption of the model is to consider a dislocation of length λ in a λ-periodic stress noise, resulting in a zero interaction energy with screw dislocations. Below we will thus only consider the case of an edge dislocation.

The link between the force- and energy-based models is that the energy variation of a dislocation segment of length λ gliding a distance w can be expressed from the work of the Peack-Koehler force in the glide plane due to the solute atoms:

$$\Delta E_p = -\int_0^w dy \int_0^\lambda dx\, b\tau_p(x,y). \tag{21}$$

This quantity is a random variable with 0 mean and variance:

$$\langle \Delta E_p^2 \rangle = b^2 \langle \tau_p^2 \rangle \int_0^w dy \int_0^w dy' \int_0^\lambda dx \int_0^\lambda dx' \Sigma(x-x', y-y'). \tag{22}$$

Assuming a λ-periodic medium along x and infinite along y and z directions as in Ref. [18], we can obtain the following analytical expression for this variance (see appendix A for details):

$$\begin{aligned}\langle \Delta E_p^2 \rangle &= b^2 \langle \tau_p^2 \rangle \lambda 30 a^3 \sqrt{\pi} \Bigg[-1 + \frac{4a^2}{w^2}\left(1 - e^{-\frac{w^2}{4a^2}}\right) \\ &\quad - \mathrm{Ei}\left(-\frac{w^2}{4a^2}\right) + \ln\left(\frac{w^2}{4a^2}\right) + \gamma_e \Bigg], \\ &= b^2 \langle \tau_p^2 \rangle \lambda a^3 \mathcal{F}(w),\end{aligned} \tag{23}$$

where $\mathrm{Ei}(x) = \int_{-\infty}^x \frac{e^u}{u} du$ and $\mathcal{F}(w)$ is a dimensionless function. We recover here the fact that $\langle \Delta E_p^2 \rangle$ is proportional to λ as obtained in Refs. [17, 18]. The term $\sqrt{\langle \Delta E_p^2 \rangle / \lambda}$ is the continuous equivalent of the quantity defined by Eq. (4) of Ref. [18].

Following the same considerations as in Ref. [18], we can use our continuous approach of the stress noise to express the energy gain for a dislocation of length L adopting a wavy shape with characteristic wavelength λ and amplitude w (equivalent to Eq. (5) of Ref. [18]):

$$\Delta E_{tot}(\lambda, w) = \left(\frac{\Gamma w^2}{2\lambda} - b\sqrt{\lambda \langle \tau_p^2 \rangle a^3 \mathcal{F}(w)} \right) \frac{L}{2\lambda} \tag{24}$$

The characteristic wavelength λ_c and amplitude w_c are then obtained at equilibrium by minimizing $\Delta E_{tot}(\lambda, w)$ with respect to λ and w, yielding:

$$\lambda_c(w) = \left(\frac{4\Gamma^2 w^4}{b^2 a^3 \langle \tau_p^2 \rangle \mathcal{F}(w)} \right)^{1/3} \tag{25}$$

and w_c solution of:

$$w_c \mathcal{F}'(w_c) = \mathcal{F}(w_c) \tag{26}$$

This last equation can be solved numerically to obtain $w_c = 5.5138a$. We find here that, as assumed *a priori* in the force-based model, w_c is a constant independent of the noise amplitude and the line tension. Numerically, this value is however about 4 times larger than assumed in the force-based model ($w_e = 1.3898a$) and is close to the minimum of the stress correlation (see Fig. 3).

Still following the same steps as in Ref. [18], we can obtain a closed-formed expression for the critical shear stress of an edge dislocation:

$$\tau_c^{energy} = 1.7294 \left(\frac{ab}{\Gamma} \right)^{1/3} \langle \tau_p^2 \rangle^{2/3}, \tag{27}$$

which can be directly compared to the prediction of the force-based model in Eq. (19). After numerical application using $w_e = 1.3898a$, the latter gives:

$$\tau_c^{force} = 1.7167 \left(\frac{ab}{\Gamma} \right)^{1/3} \langle \tau_p^2 \rangle^{2/3}. \tag{28}$$

The almost perfect numerical agreement between both expressions is fortuitous given the differences between both approaches: while the force-based model assumes a sine-shaped dislocation and performs statistics on the forces along the dislocation,

the energy-based model assumes a trapezoidal bow-out and performs statistics on the energy gained by the dislocation by bowing out, resulting in different values of both w_c, as noted above, and λ_c. It is however not surprising to find the same scaling, which can be seen as a consequence of Betti's reciprocal theorem [59]: it is equivalent (i) to look at the dislocation interacting with the stress field of the solutes as done in the force-based model and (ii) to look at the solutes interacting with the dislocation stress field as done in the energy-based model.

Determining w_c from energy considerations therefore does not modify drastically the predictions of the analytical model. However, both force- and energy-based models predict λ_c at equilibrium in absence of applied stress, while we will see in the following section that the dislocation evolves largely up to the critical stress. Also both models consider a constant value of w_c, independent of the dislocation line tension and amplitude of the stress noise, which is counter-intuitive.

B. Dislocation shape and roughening

Both force- and energy-based models presented above rely on a single length scale, λ_c that is defined at zero applied stress. However, it is well recognized that the dislocation becomes rough under applied stress with a shape that involves all length scales [10, 21]. The aim of this section is to investigate further the roughening of the dislocation under an applied stress, and to discuss the role of stress correlations on the dislocation shape. The line tension approximation is used in this section.

In Fig. 8, examples of dislocation lines are shown in the first column for the uncorrelated, edge and screw cases at zero applied stress (blue curves) and at the critical stress (red curves). As demonstrated in these pictures, the dislocation undergoes a significant roughening that seems to depend on the underlying noise environment.

To better analyse the dislocation shape, we present in the second column the power spectra averaged over 100 realizations again at zero applied stress and at the critical shear stress. With no applied stress, the dislocation simply relaxes to a local minimum and the power spectra show a characteristic wave vector marking the limit between two regimes. At large k-vectors, i.e. small wavelengths, the dislocation fluctuations are small and controlled by the dislocation stiffness. By way of contrast, at small k-vectors, i.e. long wavelengths, the dislocation can bow out significantly as the effect of the stiffness is reduced. Eventually, the amplitude reaches a value (of the order of w) where the dislocation encounters a different stress environment than for $h(x) = 0$, which balances the line tension. This translates into a saturation of the power spectra at small wave vectors visible in Fig. 8.b, d and f. The position of the cross-over between these two regimes can be associated with a characteristic length scale, which is however different from λ_c defined either through Eq. (13) or Eq. (25). Note that in the literature, λ_c is often defined through the roughness of the dislocation shape [10, 21, 40], which yields yet another potential definition of a characteristic length scale, physically and numerically different from the other definitions. Under an applied stress, the dislocations roughen progressively, resulting in an increase of the power spectra at small wave vectors in Fig. 8. For the uncorrelated case (Fig. 8.a), the power spectra converge towards a power-law behavior at the critical shear stress. This scale invariance is well documented in the framework of the depinning transition theory, with the slope of the power spectra directly related to the roughness exponent of the elastic line [21, 33]. The situation is different for edge and screw cases (Fig. 8.b and c) where the power spectra do not converge to a power law and remain concave at large wave vectors, a direct consequence of the positive correlations at short distances.

To clarify this point and further analyse the dislocation shape, one can try to derive an analytical expression for the power spectra. In the general case, this is a difficult task since the noise along the dislocation depends on both x and $h(x)$ and the final shape of the dislocation at the critical shear stress depends on the previous configurations. As a crude approximation, one can consider that the pinning stress does not depend on $h(x)$ as done in Section IV (see e.g. Eq. (14)). With this assumption, considering Eq. (4) at equilibrium yields for any $k > 0$:

$$\langle|\widehat{h}(k)|^2\rangle = \frac{b^2\langle|\widehat{\tau}_p(k)|^2\rangle}{\Gamma^2 k^4}, \tag{29}$$

with

$$\begin{aligned}\langle|\widehat{\tau}_p(k)|^2\rangle &= \frac{1}{L^2}\int_0^L\int_0^L\langle\tau_p(x)\tau_p(x')\rangle e^{ik(x-x')}dxdx' \\ &= \langle\tau_p^2\rangle\widehat{\Sigma}(k),\end{aligned} \tag{30}$$

where $\widehat{\Sigma}(k)$ is the Fourier transform of the correlation function along the dislocation direction. Considering a system L-periodic along the dislocation

direction and infinite along the other directions, Eq. (7) can be integrated along the latter to obtain in the different cases:

$$\text{uncorrelated:} \quad \widehat{\Sigma}_U(k) = \frac{\Delta x}{L}, \tag{31}$$

$$\text{edge:} \quad \widehat{\Sigma}_T(k) = \frac{15a\sqrt{\pi}}{4L}a^2k^2\left(e^{-a^2k^2}\left(1+\frac{1}{a^2k^2}\right)+(2+a^2k^2)\mathrm{Ei}(-a^2k^2)\right), \tag{32}$$

$$\text{screw:} \quad \widehat{\Sigma}_L(k) = \frac{15a\sqrt{\pi}}{L}a^2k^2\left(-e^{-a^2k^2}-(1+a^2k^2)\mathrm{Ei}(-a^2k^2)\right), \tag{33}$$

where again $\mathrm{Ei}(x) = \int_{-\infty}^{x}\frac{e^u}{u}du$. With the uncorrelated noise, $\widehat{\Sigma}_U(k)$ does not depend on the wave vector and the resulting power spectrum scales as $1/k^4$. This estimate is shown as a dashed line in Fig. 8.b and matches well the numerical power spectra obtained at τ_c. The reason is that since the noise is uncorrelated in any directions, $\tau_p(x, h(x))$ can be replaced by $\tau_p(x, 0)$ in Eq. (3) if the history dependence is neglected.

The situation is different for the edge and screw dislocations because of the noise correlations. First, the k-dependent behavior of Eq. (32-33) translates into different behaviors for the power spectra as seen in Figs. 8.d and f. In particular, in the limit of small wave vector $ka \ll 1$, we can use Taylor expansions of Eq.(32-33) to show that:

$$\langle|\widehat{h}_e(k)|^2\rangle \underset{ka\ll1}{=} \frac{15a^5b^2\langle\tau_p^2\rangle\sqrt{\pi}}{\Gamma_e^2 L}\left[\frac{1}{4a^4k^4}-\frac{\log(1/a^2k^2)-\gamma_e}{4a^2k^2}\right] \tag{34}$$

$$\langle|\widehat{h}_s(k)|^2\rangle \underset{ka\ll1}{=} \frac{15a^5b^2\langle\tau_p^2\rangle\sqrt{\pi}}{\Gamma_s^2 L}\left[\frac{-1+\log(1/a^2k^2)-\gamma_e}{a^2k^2}+(2+\log(1/a^2k^2)-\gamma_e)\right] \tag{35}$$

The theoretical power spectra of the edge dislocation recovers the $1/k^4$ power-law scaling asymptotically. It is due to the fact that on large wavelengths, the effect of the correlations along the edge dislocation are identical to an uncorrelated noise defined with a spacing $\Delta x = 15a\sqrt{\pi}/4$ as discussed in Section IV. The situation is significantly different for the screw dislocation: in the limit of small wave vectors, Eq. (35) follows a $\log(1/a^2k^2)/(a^2k^2)$ asymptotic behavior.

In contrast to the uncorrelated case, the numerical power spectra of the edge and screw dislocations do not converge towards the theoretical power spectra obtained above, as seen in Fig. 8. When the dislocation roughens and bends out of a straight line, it becomes sensitive to the 2D correlations represented in Fig. 1.a. For the edge case, the correlation spectrum is maximum along the line direction and the dislocation, after roughening away from a straight line is subjected to lower stress correlations, which explains why the theoretical power spectrum overestimates the numerical one at τ_c (see Fig. 8(d)). The situation is reversed for the screw dislocation, where the correlation spectrum is minimal along the dislocation line, resulting in an underestimation of the numerical power spectrum by the theoretical spectrum at τ_c (see Fig. 8(f)).

Therefore, at the critical shear stress, the power spectra are influenced by the anisotropic character of the stress correlations and do not follow a simple power law at small wave vectors in contrast with the general assumption in the depinning transition framework [21, 33]. In addition, while the power spectra in absence of stress reveal a characteristic wavelength, roughening under the applied stress erases this characteristic wavelength. This result seems to contradict assumptions (ii) and (iii) listed in section IV, as discussed in a recent contribution [10].

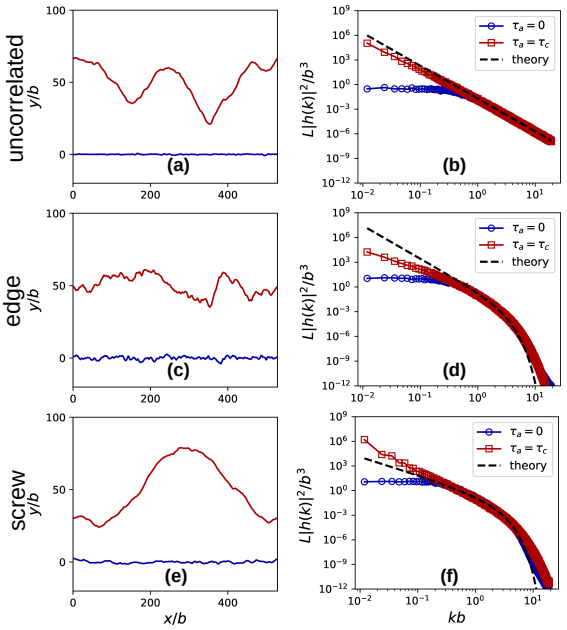

FIG. 8: Roughening of the dislocation shape between zero applied stress and the critical shear stress. The tree lines correspond respectively to the uncorrelated case (a,b), the edge case (c,d) and the edge case (e,f). Panels (a,c,e) show examples of the dislocation shape obtained at $\tau_a = 0$ (blue line) and at τ_c (red line) (for clarity reasons, the average position of both lines are arbitrarily set to $y = 0$ and $y = 50b$ respectively.). Panels (b,d,f) represent power spectra of the dislocation line also at 0 stress (blue circles) and at τ_c (red squares), compared to the theoretical estimate of Eq. (29).

CONCLUSION

In the present work, we have used a dislocation dynamics model to investigate the interactions of screw and edge dislocations with stress fields representative of random solid solutions. This was made possible thanks to the characterization of the statistical properties (variance and spatial correlations) of the shear stress field emerging from a random solid solution of dilatational solutes [41, 42]. These numerical results have been compared to the prediction of statistical models that assume that the depinning transition is controlled by a unique length-scale [15, 17, 18, 32, 33]. While this type of approach reproduces the 2/3 exponent evidenced for the edge dislocation, they fail to predict the power-law exponent evidenced for the screw dislocation. Deriving a statistical model able to predict this exponent remains an important prospect of this work.

In addition, we have studied here the extreme cases of edge and screw dislocations. The same methodology can be applied to mixed dislocations but we expect a gradual evolution with the dislocation character due to the continuous variation of the stress correlations between the transverse and longitudinal directions.

We focused here on the prediction of the critical shear stress at 0 K, without any contribution of the temperature, while most of the theories discussed above enable to derive the critical shear stress as a function of temperature [15, 17, 18]. Therefore, incorporating the role of temperature by replacing Eq. (3) with a Lanvegin dynamics constitutes a natural extension of this study that would enable to clarify the role of thermally-activated processes in dislocation motion. Note that at high temperature, solute diffusion is thermally activated and may lead to dynamical strain aging. This effect would however require a different approach than discussed here since the solutes are no longer distributed at random but segregate at the dislocation. Another limitation of our approach is the assumption of a compact core that glides with no Peierls stress. It would be valuable to incorporate dislocation dissociation by following Ref. [60] in order to investigate the role of interacting partials, the effect of their mixed character as well as the potential interference effects between the dissociation distance and the stress correlations, of the type discussed in Ref. [61]. Another perspective of this work consists in adding a periodic Peierls stress profile in order to investigate its interplay with solute strengthening. Such model would enable to discuss further the assumptions used in recent statistical models applied to dislocations in body-centered cubic concentrated alloys [62, 63].

ACKNOWLEDGMENT

AR and PAG wish to acknowledge the financial support of IDEXLYON project from the University of Lyon in the framework of the Programme Investissements dAvenir (ANR-16-IDEX-005). PAG and DR also acknowledge the support of the Agence Nationale de la Recherche through grant INSPIRA (ANR-20-CE08-0019).

Appendix A: Computing the variance $\langle \Delta E_p^2 \rangle$

Let us consider an edge dislocation oriented along the direction x and gliding in direction y. Direction z denotes the glide plane normal. As assumed in Ref. [18], we consider that the system is λ-periodic along direction x such that Eq. (22) can be written as:

$$\langle \Delta E_p^2 \rangle = b^2 \langle \tau_p^2 \rangle \lambda \int_0^w dy \int_0^w dy' \int_0^\lambda dx \Sigma(x, y - y') \quad \text{(A1)}$$

If we consider an infinite system along the y and z directions, the correlations of the resolved shear stress τ_{yz} acting on the edge dislocation can be expressed in Fourier space as (see Eq. (7)):

$$\widehat{\Sigma}(k_x, k_y, k_z) = \frac{120\pi^{3/2}a^3}{(2\pi)^2\lambda} \frac{k_y^2 k_z^2}{\boldsymbol{k}^4} e^{-a^2\boldsymbol{k}^2}, \quad \text{(A2)}$$

To obtain the correlations in the plane $z = 0$, we first integrate Eq. (A2) along the k_z direction which yields:

$$\begin{aligned} \widehat{\Sigma}(k_x, k_y) &= \int_{-\infty}^{+\infty} \widehat{\Sigma}(k_x, k_y, k_z) dk_z \\ &= \frac{60a^3\sqrt{\pi}}{2\pi\lambda} k_y^2 \left[-a\sqrt{\pi} e^{-a^2(k_x^2+k_y^2)} + \frac{\pi(1 + 2a^2(k_x^2 + k_y^2))\text{erfc}\left(a\sqrt{k_x^2 + k_y^2}\right)}{2\sqrt{k_x^2 + k_y^2}} \right] \end{aligned} \quad \text{(A3)}$$

The inner integral of Eq. (A1) can be expressed as an inverse Fourier transform of Eq. (A3) along the y direction:

$$\int_0^\lambda \Sigma(x, y) dx = \lambda \int_{-\infty}^{+\infty} \widehat{\Sigma}(k_x = 0, k_y) dk_y e^{-ik_y y} \quad \text{(A4)}$$

$$= \frac{60a^3\sqrt{\pi}}{2\pi} \int_{-\infty}^{+\infty} dk_y k_y^2 \left[-a\sqrt{\pi} e^{-a^2 k_y^2} + \frac{\pi(1 + 2a^2 k_y^2)\text{erfc}(a|k_y|)}{2|k_y|} \right] e^{-ik_y y} \quad \text{(A5)}$$

$$= 30a\sqrt{\pi} \frac{a^2}{y^2} \left[-1 + \frac{12a^2}{y^2} - e^{-y^2/4a^2} \left(2 + \frac{12a^2}{y^2} \right) \right] \quad \text{(A6)}$$

Finally, we can deduce an analytical expression for the variance $\langle \Delta E_p^2 \rangle$ by computing the double integral along the y direction of Eq. (A1), yielding Eq. (23).

[1] A. Argon, *Strengthening mechanisms in crystal plasticity*, Vol. 4 (Oxford University Press on Demand, 2008).
[2] Y. Ye, Q. Wang, J. Lu, C. Liu, and Y. Yang, Materials Today **19**, 349 (2016).
[3] E. P. George, W. Curtin, and C. C. Tasan, Acta Materialia **188**, 435 (2020).
[4] K. G. Pradeep, C. C. Tasan, M. Yao, Y. Deng, H. Springer, and D. Raabe, Materials Science and Engineering: A **648**, 183 (2015).
[5] J. Rickman, H. Chan, M. Harmer, J. Smeltzer, C. Marvel, A. Roy, and G. Balasubramanian, Nature communications **10**, 1 (2019).
[6] G. Bracq, M. Laurent-Brocq, C. Varvenne, L. Perrière, W. Curtin, J.-M. Joubert, and I. Guillot, Acta Materialia **177**, 266 (2019).
[7] S. Patinet and L. Proville, Physical Review B **78**, 104109 (2008).
[8] S. Patinet, D. Bonamy, and L. Proville, Physical Review B **84**, 174101 (2011).
[9] S. Patinet and L. Proville, Philosophical Magazine **91**, 1581 (2011).
[10] G. Péterffy, P. D. Ispánovity, M. E. Foster, X. Zhou, and R. B. Sills, Materials Theory **4**, 1 (2020).

[11] R. B. Sills, M. E. Foster, and X. W. Zhou, International Journal of Plasticity **135**, 102791 (2020).
[12] J. Friedel, *Dislocations: International Series of Monographs on Solid State Physics*, Vol. 3 (Elsevier, 2013).
[13] R. Fleischer, Acta Metallurgica **9**, 996 (1961).
[14] N. Mott and F. Nabarro, "Report conf. on the strength of solids, bristol," (1948).
[15] R. Labusch, Physica Status Solidi (b) **41**, 659 (1970).
[16] F. Nabarro, Philosophical Magazine **35**, 613 (1977).
[17] G. P. M. Leyson, W. A. Curtin, L. G. Hector, and C. F. Woodward, Nature Materials **9**, 750 (2010).
[18] C. Varvenne, A. Luque, and W. A. Curtin, Acta Materialia **118**, 164 (2016).
[19] C. Varvenne and W. A. Curtin, Scripta Materialia **142**, 92 (2018).
[20] C. R. LaRosa, M. Shih, C. Varvenne, and M. Ghazisaeidi, Materials Characterization **151**, 310 (2019).
[21] A.-L. Barabási, H. E. Stanley, *Fractal concepts in surface growth* (Cambridge university press, 1995).
[22] M. Kardar, G. Parisi, and Y.-C. Zhang, Physical Review Letters **56**, 889 (1986).
[23] N. Martys, M. Cieplak, and M. O. Robbins, Physical Review Letters **66**, 1058 (1991).
[24] S. Patinet, D. Vandembroucq, and S. Roux, Physical Review Letters **110**, 165507 (2013).
[25] T. Nattermann, S. Stepanow, L.-H. Tang, and H. Leschhorn, Journal de Physique II **2**, 1483 (1992).
[26] L. A. N. Amaral, A.-L. Barabási, and H. E. Stanley, Physical Review Letters **73**, 62 (1994).
[27] Z. Olami, I. Procaccia, and R. Zeitak, Physical Review E **52**, 3402 (1995).
[28] A. Rosso, A. K. Hartmann, and W. Krauth, Physical Review E **67**, 021602 (2003).
[29] C. J. Bolech and A. Rosso, Physical Review Letters **93**, 125701 (2004).
[30] O. Duemmer and W. Krauth, Physical Review E **71**, 061601 (2005).
[31] A. B. Kolton, A. Rosso, E. V. Albano, and T. Giamarchi, Physical Review B **74**, 140201 (2006).
[32] A. Larkin and Y. Ovchinnikov, Journal of Low Temperature Physics **34**, 409 (1979).
[33] S. Zapperi and M. Zaiser, Materials Science and Engineering: A **309**, 348 (2001).
[34] K. Park and I.-m. Kim, Journal of the Physical Society of Japan **72**, 111 (2003).
[35] E. Medina, T. Hwa, M. Kardar, and Y.-C. Zhang, Physical Review A **39**, 3053 (1989).
[36] J. G. Amar, P.-M. Lam, and F. Family, Physical Review A **43**, 4548 (1991).
[37] C.-H. Lam, L. M. Sander, and D. E. Wolf, Physical Review A **46**, R6128 (1992).
[38] M.-P. Kuittu, M. Haataja, and T. Ala-Nissila, Physical Review E **59**, 2677 (1999).
[39] H. Janssen, U. C. Täuber, and E. Frey, The European Physical Journal B-Condensed Matter and Complex S
[40] J.-H. Zhai and M. Zaiser, Materials Science and Engineering: A **740**, 285 (2019).
[41] P.-A. Geslin and D. Rodney, Journal of the Mechanics and Physics of Solids **153**, 104479 (2021).
[42] P.-A. Geslin, A. Rida, and D. Rodney, Journal of the Mechanics and Physics of Solids **153**, 104480 (2021).
[43] H. S. Oh, D. Ma, G. P. Leyson, B. Grabowski, E. S. Park, F. Körmann, and D. Raabe, Entropy **18**, 321 (2016).
[44] O. N. Senkov, D. B. Miracle, K. J. Chaput, and J.-P. Couzinie, Journal of Materials Research **33**, 3092 (2018).
[45] A. Lemaître, The Journal of Chemical Physics **149**, 104107 (2018).
[46] W. Cai, A. Arsenlis, C. R. Weinberger, and V. V. Bulatov, Journal of the Mechanics and Physics of Solids **54**, 561 (2006).
[47] P.-A. Geslin and D. Rodney, Physical Review B **98**, 174115 (2018).
[48] H. Dammak, Y. Chalopin, M. Laroche, M. Hayoun, and J.-J. Greffet, Physical Review Letters **103**, 190601 (2009).
[49] F. Brieuc, Y. Bronstein, H. Dammak, P. Depondt, F. Finocchi, and M. Hayoun, Journal of chemical theory and computation **12**, 5688 (2016).
[50] T. Nogaret and D. Rodney, Physical Review B **74**, 134110 (2006).
[51] B. Bakó, D. Weygand, M. Samaras, W. Hoffelner, and M. Zaiser, Physical Review B **78**, 144104 (2008).
[52] X.-Y. Liu and J. B. Adams, Acta Materialia **46**, 3467 (1998).
[53] S. Plimpton, Journal of Computational Physics **117**, 1 (1995).
[54] V. Podkuyko and V. Pustovalov, Cryogenics **18**, 589 (1978).
[55] G. Salishchev, M. Tikhonovsky, D. Shaysultanov, N. Stepanov, A. Kuznetsov, I. Kolodiy, A. Tortika, and O. Senkov, Journal of Alloys and Compounds **591**, 11 (2014).
[56] J. Hirth and J. Lothe, *Theory of Dislocations* (McGraw-Hill, New York, 1968).
[57] W. G. Nöhring and W. Curtin, Acta Materialia **128**, 135 (2017).
[58] L. Proville and S. Patinet, Physical Review B **82**, 054115 (2010).
[59] E. Betti, Il Nuovo Cimento (1869-1876) **7**, 158 (1872).
[60] P.-A. Geslin and D. Rodney, Modelling and Simulation in Materials Science and Engineering **28**, 0
[61] W. Cai, V. V. Bulatov, J. F. Justo, A. S. Argon, and S. Yip, Physical Review Letters **84**, 3346 (2000).
[62] F. Maresca and W. A. Curtin, Acta Materialia **182**, 235 (2020).
[63] F. Maresca and W. A. Curtin, Acta Materialia **182**, 144 (2020).